This CVPR 2021 workshop paper is the Open Access version, provided by the Computer Vision Foundation.
Except for this watermark, it is identical to the accepted version;
the final published version of the proceedings is available on IEEE Xplore.

An Infrared Thermography Model Enabling Remote Body Temperature Screening Up to 10 Meters

Jing Wei Chin[1,2*], Kwan Long Wong[1,2*], Tsz Tai Chan[1,2], Kristian Suhartono[1], Richard H.Y. So[1,2]

[1]The Hong Kong University of Science and Technology, [2]PanopticAI Ltd.

Abstract

During the COVID-19 pandemic, temperature screening has emerged as a common practice in the infection control pipeline. In particular, thermal imaging systems have risen in popularity for preliminary screening of individuals with elevated temperatures, especially in high throughput areas. However, remote temperature measurement is intrinsically complex and susceptible to unavoidable influences from the measuring environment. We study the effects of sensor-subject distance on remote temperature readings and present an infrared-based system for rapid temperature screening over long distances (2 m to 10 m). The system applies a state-of-the-art pose estimation algorithm to extract the face box locations, sensor-subject distances, and facial temperatures within a scene. For the use of infrared thermography in humans, we propose a thermal compensation model to correct the temperature of subjects measured at different distances and perform analyses to evaluate the trade-off between missing rate (elevated temperature does not trigger an alarm) and false alarm rate (normal temperature triggers an alarm). The experimental results show our system's promise to identify subjects with elevated temperatures and the potential to improve temperature screening protocols in different environments.

1. Introduction

Temperature screening practices have been widely adopted to help control and prevent the spread of infectious diseases such as Severe Acute Respiratory Syndrome (SARS), Ebola, swine influenza, and the novel coronavirus (COVID-19). Amid the COVID-19 pandemic, health authorities recommend facilities (*e.g.*, airports, stations, malls, offices, schools, hospitals, etc.) to closely monitor the body temperature of incoming personnel and segregate those who show symptoms indicative of fever (*e.g.*, above 37.5°C) [16]. In high throughput areas, the ideal temperature screening solution should be non-invasive, fast, provide a safe physical distance (2 m) between the operator and the subject, and sufficiently accurate in identifying elevated temperatures while minimizing any inconvenience to human traffic.

When used for an initial temperature assessment, thermal imaging systems have shown significant promise for mass temperature screening since the SARS outbreak in 2003 [1, 15, 4]. Thermal cameras can detect and measure infrared radiation emitted by an object, which offers a non-contact method to determine a person's surface skin temperature in real-time. However, conventional systems often require well-trained human operators to closely monitor the thermal images [14]. For many thermal imaging systems that include a color camera component, the operator also needs to manually check between the thermal and color images to identify a suspect with elevated temperature. This process is tedious, prone to human errors especially at long distances and varying environments, and susceptible to false-positive readings from heated background objects (*e.g.*, hot coffee).

Given the widespread usage of thermal imaging systems in different environments, it's critical to assess the potential factors that influence the reliability of remote temperature measurements [5]. Most notably, the distance between the thermal sensor and the target (sensor-subject distance) is known to contribute to measurement uncertainty [6, 24]. While adjusting the threshold temperature value can serve as a temporary solution, it is not generalizable for moving subjects across larger areas. Without using a depth camera, there is also an added difficulty to first estimate the distance of a subject detected in the real-world 3D environment from a 2D color image [10]. For infrared thermography in human temperature screening applications, accurate compensation of the effects from the sensor-subject distance is essential.

Recently, deep learning techniques have achieved state-of-the-art results in many computer vision applications. In particular, the developments in multi-person human pose estimation techniques enable accurate localization of face, body, hands, and feet keypoints simultaneously [2, 3]. In a

*Joint first authors ({jwchin, klwongaz}@connect.ust.hk)

temperature screening context, this technology can be applied for mass human detection at long distances and analytics of body proximity information to locate the corresponding regions for temperature measurement (*e.g.*, inner canthi and forehead).

This paper presents an infrared-based system for real-time temperature screening over long distances. The proposed system detects whole-body keypoints within a color image and simultaneously maps the coordinates to the corresponding thermal image to capture temperature information within a region of interest. We evaluate the influence of subject-sensor distance and propose a dynamic compensation algorithm to improve measurement accuracy. Finally, we test the system's ability to classify subjects with elevated temperatures among a large moving crowd. When used as the first line of defense, the system shows promise for mass temperature screening.

2. Related Works

Lahiri *et al*. [11] presented a comprehensive review of infrared thermography in medical applications, which includes fever screening with conventional thermal imaging systems. Ghassemi and colleagues [9] suggested methods to optimize performance and testing for thermographic fever screening. Lin *et al*. [12] proposed a continuous body temperature measurement system using a low-cost and low-resolution thermal camera (FLIR Lepton 2.5). Their deep learning-based method adapted the MobileNet-SSD architecture to perform face detection in thermal images followed by temperature measurement of the subject's forehead area. However, their approach was limited to a single user and only validated on stationary subjects. The group of Sumriddetchkajorn [20] proposed a mobile-platform module that can screen the temperature of up to nine people simultaneously. Using a low-cost FLIR One camera, their solution included an offset temperature module to compensate for ambient temperature fluctuations. Although they demonstrated promising results in a field test, subjects were required to pause for 5 seconds at a predefined distance in front of the camera to obtain facial temperature measurements. Other studies have proposed temperature screening systems that include features like a disinfection sterilization component [17] or the detection of additional vital signs [13, 21] to improve the odds of combating infectious diseases. Nonetheless, existing studies all focus on temperature measurement at fixed and short distances.

3. Methods

3.1. System Implementation

The proposed system hardware included a camera unit, an environmental sensor, and a computing unit (Intel Core i9 and NVIDIA RTX 2080 Ti). The camera unit consisted of a Logitech BRIO color camera mounted 73mm below a FLIR E8-XT thermal camera and placed at the height of 2.3m with a tilting angle of 17 degrees below the horizontal. The color images were spatially registered to the thermal images using the homography transformation described by Dubrofsky *et al*. [7].

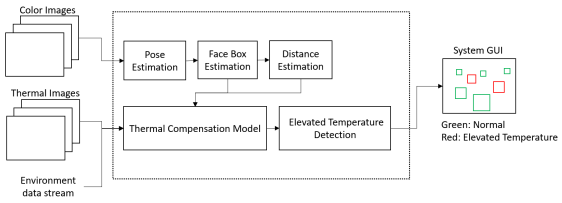

Figure 1. Schematic diagram of data processing pipeline for predicting suspects with elevated temperature within a frame.

Figure 1 presents an overview of the data processing pipeline that occurs on each frame captured by our system. Firstly, the OpenPose real-time multi-person 2D pose estimation algorithm [2, 19] was applied to obtain all human keypoints in the color image. Since the resolution of the color image (3840 x 2160 pixels) is much higher than that of the thermal image (320 x 240 pixels), processing on the color image enables more accurate keypoint detection at longer distances. Based on upper body keypoint information, the face box coordinates of each detected human were estimated and used to predict the sensor-subject distance. Next, the thermal image, corresponding face box coordinates, sensor-subject distance, and ambient temperature reading were input into our thermal compensation model to estimate the corrected temperature values within each face box. Finally, temperature status was evaluated based on an alarm threshold and depicted as a green (normal temperature) or red (elevated temperature) face box on the color image.

3.2. Sensor-Subject Distance Estimation

With the assumption that all subjects within a scene are standing on the same planar floor, the sensor-subject distance, d, can be estimated by a reciprocal function of the size of a subject's face box as:

$$d = \frac{a}{s - h} + k \tag{1}$$

where s denotes the diagonal pixel length of the subject's face box and a, h and k are estimated constants.

N = 366 measurements of the size of human face boxes at different distances (2 m to 11 m) were collected in 1-meter increments. The sensor-subject distance was plotted against the mean diagonal length of face boxes at each distance and non-linear least squares was used to fit Equation 1 to the data (Figure 3).

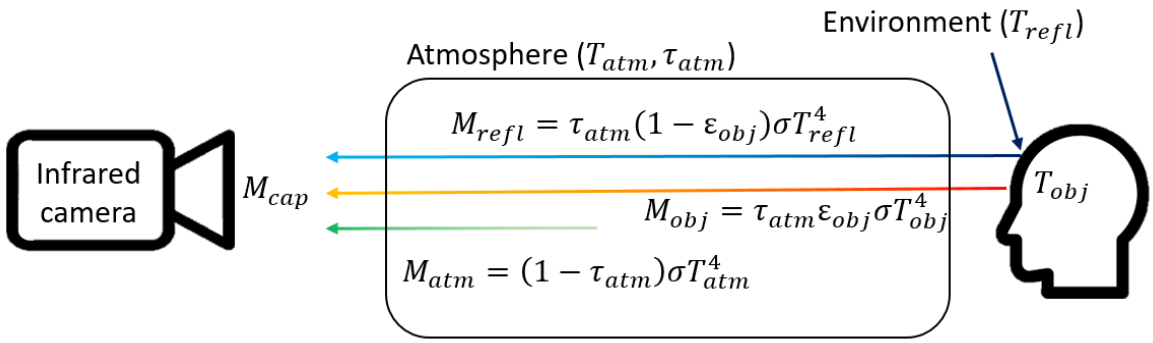

Figure 2. Schematic diagram of the total radiant emittance captured by an infrared camera screening a subject.

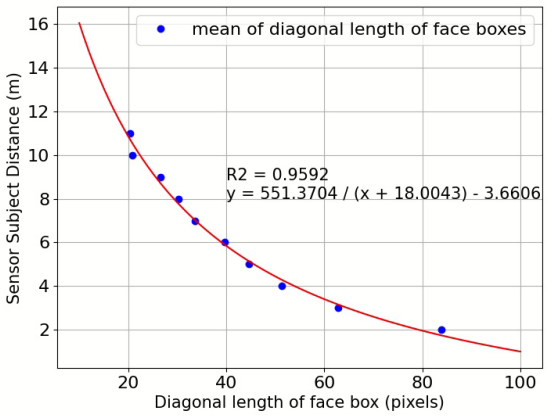

Figure 3. Plot of sensor-subject distance versus the diagonal length of the subject's face box.

Subsequently, the subject-sensor distance d can be estimated by:

$$d = \frac{551.3704}{s + 18.0043} - 3.6606 \tag{2}$$

3.3. Thermal Compensation Model

According to the Stefan-Boltzmann Law, the radiant emittance of an object (M) is:

$$M = \varepsilon\sigma T^4 \tag{3}$$

where ε is the emissivity of the object, σ is the Stefan-Boltzmann constant and T is the temperature of the object.

For remote temperature measurement of an object using infrared thermography, a general model of the total radiant emittance captured by an infrared camera is illustrated in Figure 2. The total radiant emittance (M_{cap}) captured by an infrared camera is:

$$M_{cap} = M_{obj} + M_{refl} + M_{atm} \tag{4}$$

where M_{obj} is the radiant emittance of the object, M_{refl} is the radiant emmitance of the surroundings reflected by the object and M_{atm} is the radiant emmitance of the atmosphere. The transmittance of the atmosphere (τ_{atm}) describes the efficiency of radiant emittance transmitted through the atmosphere, which is considered by M_{obj} and M_{refl}. Hence, the emissivity (emittance) of the atmosphere is $1 - \tau_{atm}$ and substituting the terms into Equation 4 yields [23]:

$$\begin{aligned} M_{cap} = \tau_{atm}\varepsilon_{obj}\sigma T_{obj}^4 + \tau_{atm}(1 - \varepsilon_{obj})\sigma T_{refl}^4 \\ + (1 - \tau_{atm})\sigma T_{atm}^4 \end{aligned} \tag{5}$$

Most cameras do not have the capability to measure the transmittance of the atmosphere. When an object to be measured is at a close distance, τ_{atm} can be assumed equal to 1, and Equation 5 simplifies to:

$$M_{cap} = \varepsilon_{set}\sigma T_o^4 + (1 - \varepsilon_{set})\sigma T_{set}^4 \tag{6}$$

where ε_{set} is the object's emissivity set in the camera (0.98 by default), T_o is the object's raw temperature measured by the camera, and T_{set} is the reflected temperature of the surroundings set in the camera (293.15°K by default).

The estimated temperature of the object, $\hat{T}_{obj}$, is obtained by rearranging Equation 5 and substituting parameters with our estimated values:

$$\hat{T}_{obj} = \left(\frac{M_{cap} - \hat{M}_{atm} - \hat{M}_{refl}}{\hat{\tau}_{atm}\varepsilon_{obj}\sigma}\right)^{\frac{1}{4}} \tag{7}$$

where ε_{obj} is the object's emissivity (assumed to be 0.969 for the human forehead [22]), $\hat{M}_{atm}$ is estimated from the ambient temperature sensor reading T_{amb} as:

$$\hat{M}_{atm} = (1 - \hat{\tau}_{atm})\sigma T_{amb}^4 \tag{8}$$

$\hat{M}_{refl}$ is estimated by assuming T_{refl} equals T_{amb} as:

$$\hat{M}_{refl} = \hat{\tau}_{atm}(1 - \varepsilon_{obj})\sigma T_{amb}^4 \tag{9}$$

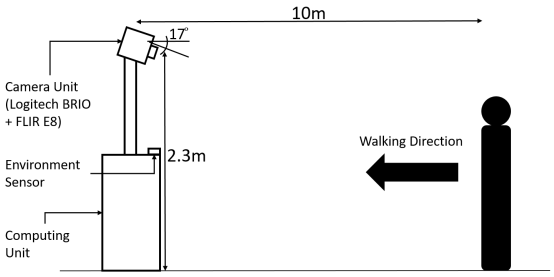

Figure 4. Illustration of experimental setup.

and $\hat{\tau}_{atm}$ is estimated by the sensor-subject distance [18] such that:

$$\hat{\tau}_{atm} = e^{-a_1(\sqrt{\hat{d}}-\sqrt{d_{cal}})-a_2(\hat{d}-d_{cal})} \tag{10}$$

where a_1 and a_2 are the estimated coefficients affected by the environment atmosphere, $\hat{d}$ is the estimated sensor-subject distance, d_{cal} is the calibration distance (assumed to be 0).

In order to account for the influence of factors unaddressed by the traditional thermography model, the compensated temperature, T'_{obj}, can be calculated as:

$$T'_{obj} = \hat{T}_{obj} + a_3\hat{d} + a_4 \tag{11}$$

where a_3 is the estimated coefficient related to the distance, such as low thermal image resolution and out of focus at long distances, and a_4 is the estimated coefficient for other uncontrolled factors like hardware calibration error and environmental factors [8, 5].

4. Experiments and Results

4.1. Experimental Setup and Protocol

The experiment was conducted with 8 healthy subjects (5 males and 3 females). An overview of the experimental setup is illustrated in Figure 4. Each subject stood front facing our system at 9 different sensor-subject distances (2 m to 10 m in 1-meter increments). At each sensor-subject distance, the subject's forehead temperature was measured by our system and 3 times with a handheld thermometer (functional equivalent to those used in border control points (EF-24R3 or EF-23R300 from Medisuper)). This process was conducted once with the subject's normal forehead temperature and again with an elevated forehead temperature. Elevated forehead temperature was simulated by putting a hot pack on the subject's forehead for 10 seconds before the temperature measurement.

The range of forehead temperatures of normal subjects is between $36.2°C$ and $36.7°C$ with a mean of $36.5°C$ and the range of simulated elevated temperatures is between

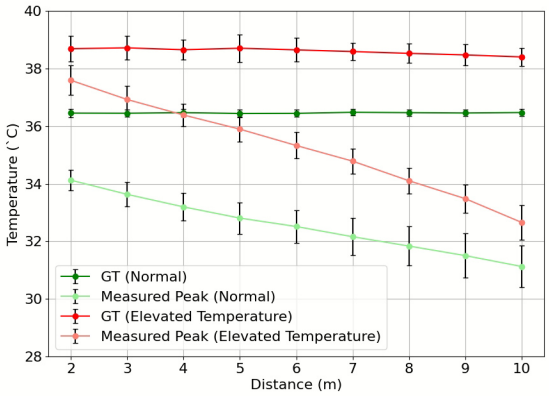

Figure 5. Raw data of normal and elevated forehead temperatures measured by handheld thermometer (GT) and thermal camera (Measured Peak) at sensor-subject distances of 2 m to 10 m.

$38°C$ and $39.7°C$ with a mean of $38.6°C$. The mean ambient temperature throughout the experiment is $23.46°C$ with S.D. of $0.05°C$ and the mean humidity is 77.62% with S.D. of 0.25%. Figure 5 shows the raw data captured by the thermal camera (Measured Peak) and handheld thermometer (GT) at various distances.

4.2. Experimental Results

The Pearson correlation coefficient (PCC), average mean absolute error (MAE), and average root-mean-square error (RMSE) are utilized to compare the results between the raw temperature measured by the thermal camera before compensation and the temperature by our system after compensation. As illustrated in Table 1, the PCC increased by 0.1814, MAE decreased by $3.053°C$, and RMSE decreased by $3.004°C$ after temperature compensation.

	PCC	MAE ($°C$)	RMSE ($°C$)
Before	0.7481	3.641	3.681
After	0.9295	0.588	0.677

Table 1. Comparison of Pearson correlation coefficient (PCC), average mean absolute error (MAE) and average root-mean-square error (RMSE) before and after thermal compensation. The results after compensation show significant improvement.

4.3. Elevated Temperature Classification

Figure 6 shows the 10-fold cross-validation results of elevated temperature classification accuracy at different sensor-subject distances. The alarm threshold that classifies a subject as having an elevated temperature was set to $37.5°C$ (*i.e.*, a temperature reading above $37.5°C$ signals the alarm). The results show that our system with thermal compensation achieves perfect classification accuracy from 2 m to 7 m and above 80% at 9 m.

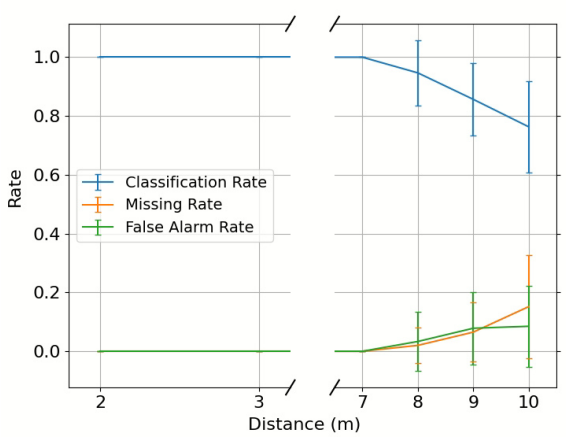

Figure 6. 10-fold cross validation of elevated temperature classification rate, missing rate (subject has elevated temperature and does not trigger the alarm) and false alarm rate (subject has normal temperature and triggers the alarm) of our system after thermal compensation from 2 m to 10 m. The alarm threshold was set to 37.5°C.

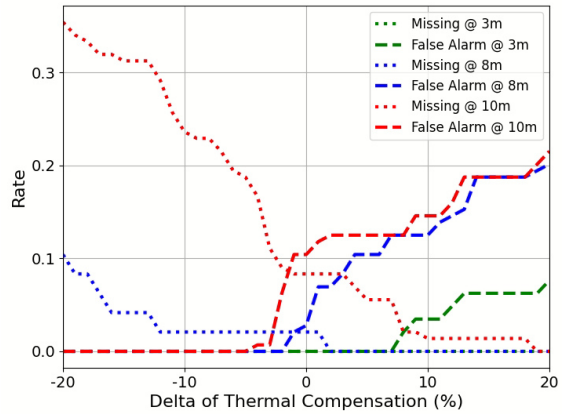

Figure 7. Sensitivity analysis of our thermal compensation model at sensor-subject distance of 3 m, 8 m and 10 m. There is a trade-off between missing rate and false alarm rate.

Given the wide variety of individual, technical and environmental factors that can influence the interpretation of thermal images [8, 5], we observe a trade-off between missing rate and false alarm rate especially at further distances (8 m - 10 m). Figure 7 shows a sensitivity analysis of the thermal compensation value predicted by our model at sensor-subject distance of 3 m, 8 m and 10 m. The thermal compensation value is obtained by rewriting Equation 11 as:

$$T'_{obj} = T_o + T_{comp} \tag{12}$$

where T_o is the raw temperature measurement from the thermal camera and T_{comp} is the thermal compensation value predicted by our model which includes all the corrections for the camera parameters and distance effect. Then α is added into equation to control the strength of the thermal compensation:

$$T'_{obj} = T_0 + \alpha * T_{comp} \tag{13}$$

The delta of thermal compensation is defined as $(\alpha - 1)$ and used for the sensitivity analysis.

4.4. Alarm Threshold Analysis

Figure 8 illustrates an analysis of elevated temperature alarm thresholds on average classification rate at different sensor-subject distances before and after thermal compensation. Before applying our thermal compensation model, the highest average classification rate is 82.25% at an alarm threshold of 33.9°C. While it is still possible to achieve

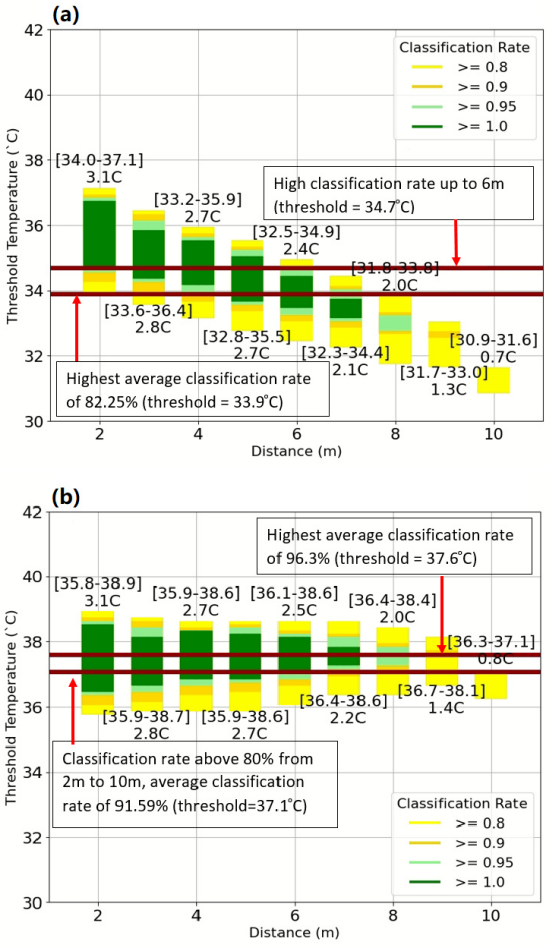

Figure 8. Elevated temperature alarm threshold analysis (a) before applying thermal compensation (b) after applying thermal compensation. The average classification rate increases significantly and a single threshold is capable of achieving a classification rate above 80% across all sensor-subject distances.

good performance at closer sensor-subject distances (2 m to 5 m) when the alarm threshold is set to 34.7°C, the classification rate significantly decreases when the sensor-subject distance is greater than 5 m. After applying our thermal compensation algorithm, the average classification rate increases significantly by 14.05% when the alarm threshold is set to 37.6°C. Although perfect classification of elevated temperature remains to be challenging especially at longer sensor-subject distances (8 m to 10 m), our system can achieve a classification rate above 80% at all sensor-subject distances when the alarm threshold is set to 37.1°C.

4.5. Multi-person Load Test

Our system's performance was evaluated on a private data set containing subjects with simulated elevated temperature walking among a large moving crowd. When used in a practical setting, the system's graphic user interface indicates temperature status by depicting green (normal temperature) or red (elevated temperature) face boxes on the color image. Choosing a suitable alarm threshold to balance missing and false alarm rates should be thoroughly considered before deployment. For illustration purposes and to maintain data privacy, only the red face boxes overlaid on the thermal image are shown in this paper. As seen in Figure 9, our system with thermal compensation successfully identifies the two subjects with elevated temperature (at different sensor-subject distances) simultaneously. The preliminary results point towards promising applications for mass temperature screening.

Figure 9. Thermal image of a crowd walking past our system where two subjects at different sensor-subject distances have simulated elevated forehead temperature. After thermal compensation, our system successfully identified the two subjects (red boxes) in real-time using a single alarm threshold.

5. Conclusion

In this paper, we propose an infrared-based system for remote temperature screening over long distances. We study the effects of sensor-subject distance and present a thermal compensation model to correct factors unaddressed by traditional thermography. The experimental results show significant improvement in temperature measurement after compensation, increasing the PCC by 0.1814 and decreasing the average MAE and average RMSE by $3.053°C$ and $3.004°C$ respectively. We perform a sensitivity analysis to observe the trade-off between the missing rate and false alarm rate. We further demonstrate that our system can identify subjects with elevated temperature at different sensor-subject distances among a moving crowd of more than 20 people. The preliminary results suggest our system's promise for large-scale temperature screening applications.

Future work involves validating our system in different environments and further investigation of other variables that influence infrared thermography for human temperature screening. The effects of environmental factors, such as ambient temperature and humidity, and technical factors like hardware constraints from thermal image resolution and lens focus are currently being studied.

Acknowledgement

This work is partially funded by BGF0041920 and SST18220GP. We are grateful for the support from the University Grants Committee and Innovation and Technology Commission of Hong Kong.

References

[1] David M Bell. Public health interventions and sars spread, 2003. *Emerging Infectious Diseases*, 10(11):1900, 2004.

[2] Zhe Cao, Gines Hidalgo, Tomas Simon, Shih-En Wei, and Yaser Sheikh. Openpose: realtime multi-person 2d pose estimation using part affinity fields. *IEEE Transactions on Pattern Analysis and Machine Intelligence*, 43(1):172–186, 2019.

[3] Yucheng Chen, Yingli Tian, and Mingyi He. Monocular human pose estimation: A survey of deep learning-based methods. *Computer Vision and Image Understanding*, 192:102897, 2020.

[4] Ming-Fu Chiang, Po-Wei Lin, Li-Fong Lin, Hung-Yi Chiou, Ching-Wen Chien, Shu-Fen Chu, and Wen-Ta Chiu. Mass screening of suspected febrile patients with remote-sensing infrared thermography: alarm temperature and optimal distance. *Journal of the Formosan Medical Association*, 107(12):937–944, 2008.

[5] Giovanni Battista Dell'Isola, Elena Cosentini, Laura Canale, Giorgio Ficco, and Marco Dell'Isola. Noncontact body temperature measurement: Uncertainty evaluation and screening decision rule to prevent the spread of covid-19. *Sensors*, 21(2):346, 2021.

[6] David P DeWitt and Gene D Nutter. *Theory and practice of radiation thermometry*. John Wiley & Sons, 1988.

[7] Elan Dubrofsky. Homography estimation. *Diplomová práce. Vancouver: Univerzita Britské Kolumbie*, 5, 2009.

[8] Ismael Fernández-Cuevas, Joao Carlos Bouzas Marins, Javier Arnáiz Lastras, Pedro María Gómez Carmona, Sergio Piñonosa Cano, Miguel Ángel García-Concepción, and Manuel Sillero-Quintana. Classification of factors influencing the use of infrared thermography in humans: A review. *Infrared Physics & Technology*, 71:28–55, 2015.

[9] Pejman Ghassemi, T Joshua Pfefer, Jon P Casamento, Rob Simpson, and Quanzeng Wang. Best practices for standardized performance testing of infrared thermographs intended for fever screening. *PLOS One*, 13(9):e0203302, 2018.

[10] Faisal Khan, Saqib Salahuddin, and Hossein Javidnia. Deep learning-based monocular depth estimation methods—a state-of-the-art review. *Sensors*, 20(8):2272, 2020.

[11] BB Lahiri, S Bagavathiappan, T Jayakumar, and John Philip. Medical applications of infrared thermography: a review. *Infrared Physics & Technology*, 55(4):221–235, 2012.

[12] Jia-Wei Lin, Ming-Hung Lu, and Yuan-Hsiang Lin. A thermal camera based continuous body temperature measurement system. In *Proceedings of the IEEE/CVF International Conference on Computer Vision Workshops*, pages 0–0, 2019.

[13] Toshiaki Negishi, Shigeto Abe, Takemi Matsui, He Liu, Masaki Kurosawa, Tetsuo Kirimoto, and Guanghao Sun. Contactless vital signs measurement system using rgb-thermal image sensors and its clinical screening test on patients with seasonal influenza. *Sensors*, 20(8):2171, 2020.

[14] Eddie YK Ng and Rajendra U Acharya. Remote-sensing infrared thermography. *IEEE Engineering in Medicine and Biology Magazine*, 28(1):76–83, 2009.

[15] Eddie YK Ng, GJL Kawb, and WM Chang. Analysis of ir thermal imager for mass blind fever screening. *Microvascular Research*, 68(2):104–109, 2004.

[16] World Health Organization et al. Rational use of personal protective equipment for coronavirus disease (covid-19): interim guidance, 27 february 2020. Technical report, World Health Organization, 2020.

[17] Sivajothi Paramasivam, Chua Huang Shen, Alireza Zourmand, Amira Kamil Ibrahim, Ahmed Mohamed Alhassan, and Abdelwhab Faroug Eltirifl. Design and modeling of iot ir thermal temperature screening and uv disinfection sterilization system for commercial application using blockchain technology. In *2020 IEEE 10th International Conference on System Engineering and Technology (ICSET)*, pages 250–255. IEEE, 2020.

[18] Slavko Pokorni. Error analysis of surface temperature measurement by infrared sensor. *International Journal of Infrared and Millimeter Waves*, 25:1523–1533, 10 2004.

[19] Tomas Simon, Hanbyul Joo, Iain Matthews, and Yaser Sheikh. Hand keypoint detection in single images using multiview bootstrapping. In *Proceedings of the IEEE conference on Computer Vision and Pattern Recognition*, pages 1145–1153, 2017.

[20] Armote Somboonkaew, Sirajit Vuttivong, Panintorn Prempree, Ratthasart Amarit, Sataporn Chanhorm, Kosom Chaitavon, Supanit Porntheeraphat, and Sarun Sumriddetchkajorn. Temperature-compensated infrared-based low-cost mobile platform module for mass human temperature screening. *Applied Optics*, 59(17):E112–E117, 2020.

[21] Guanghao Sun, Yosuke Nakayama, Sumiyakhand Dagdanpurev, Shigeto Abe, Hidekazu Nishimura, Tetsuo Kirimoto, and Takemi Matsui. Remote sensing of multiple vital signs using a cmos camera-equipped infrared thermography system and its clinical application in rapidly screening patients with suspected infectious diseases. *International Journal of Infectious Diseases*, 55:113–117, 2017.

[22] T Togawa. Non-contact skin emissivity: measurement from reflectance using step change in ambient radiation temperature. *Clinical physics and physiological measurement : an official journal of the Hospital Physicists' Association, Deutsche Gesellschaft fur Medizinische Physik and the European Federation of Organisations for Medical Physics*, 10(1):39—48, February 1989.

[23] Rubén Usamentiaga, Pablo Venegas, Jon Guerediaga, Laura Vega, Julio Molleda, and Francisco G Bulnes. Infrared thermography for temperature measurement and non-destructive testing. *Sensors*, 14(7):12305–12348, 2014.

[24] Nina Zaproudina, Ville Varmavuo, Olavi Airaksinen, and Matti Närhi. Reproducibility of infrared thermography measurements in healthy individuals. *Physiological Measurement*, 29(4):515, 2008.